Rocznik Ochrona Środowiska

Volume 27 Year 2025 ISSN 2720-7501 pp. 582-598

https://doi.org/10.54740/ros.2025.047 open access

Received: July 2025 Accepted: September 2025 Published: October 2025

Biotechnological Evaluation and Predictive Modeling of Bio-Based Adsorbents for Turquoise Blue Dye Detoxification: Integrating Experimental Validation and Machine Learning

Malarvizhi Thangaraj[1], Saveeth Ramanathan[2], Angeline Kiruba Dunston[3]*

[1]Department of Industrial Biotechnology, Government College of Technology, Coimbatore, Tamil Nadu, India

[2]Department of Computer Science and Engineering,
Coimbatore Institute of Technology, Coimbatore, Tamil Nadu, India
https://orcid.org/0000-0003-2387-0271

[3]Department of Industrial Biotechnology, Government College of Technology, Coimbatore, Tamil Nadu, India

[*]corresponding author's e-mail: saveeth.r@cit.edu.in

Abstract: This study presents a data-driven hybrid framework that combines experimental adsorption trials with machine learning and evolutionary optimization to enhance the removal of Turquoise Blue Dye from aqueous media. Three bio-adsorbents, Azadirachta indica, Phyllanthus emblica, and Saraca asoca, and their equi-mass mixture were examined for synergistic adsorption performance. Batch experiments were conducted by varying the pH (3-11), contact time (20-120 minutes), dye concentration (20-120 ppm), and adsorbent dosage (0.02-0.1 g/L). The composite mixture achieved the highest removal efficiency at 77% exceeding *Phyllanthus emblica* at 74%, *Saraca asoca* at 70%, and *Azadirachta indica* at 63.8%. FTIR analysis confirmed chemical interactions via hydroxyl, carboxyl and carbonyl groups. Supervised models, including Random Forest with a coefficient of determination of 0.92 and mean squared error of 0.0021, were optimized using Differential Evolution. This integrative strategy supports scalable and intelligent solutions for industrial dye effluent remediation.

Keywords: bio-adsorbents, turquoise blue dye removal, machine learning regression models

1. Introduction

Dyes are extensively utilized across various industrial sectors, including textile manufacturing, paper production, plastics, and leather processing, resulting in the generation of substantial volumes of dye-laden effluents (Periyasamy 2024). With an annual global production exceeding 1.6 million tons, approximately 10-15% of dyes are released into the environment as untreated or partially treated industrial wastewater (Dutta et al. 2024). These effluents are characterized by the persistence of synthetic dyes, which exhibit high chemical stability, poor biodegradability, and inherent toxicity. Consequently, their accumulation in aquatic ecosystems leads to severe ecological disturbances including photoinhibition decreased dissolved oxygen levels and disruption of aquatic biodiversity (Islam et al. 2025, Khandelwal Rana et al. 2024). Moreover, chronic exposure to these contaminants has been associated with adverse human health effects such as dermatological disorders, respiratory ailments, mutagenic transformations, and carcinogenic outcomes (Montano et al. 2025). To address the environmental risks of dye pollution, remediation strategies such as coagulation, oxidation, membrane filtration, and biodegradation have been explored. Adsorption has emerged as the most effective due to its simplicity, cost-efficiency, and high removal rates (Kamati et al. 2024). However, the high cost of commercial adsorbents, such as activated carbon, has prompted interest in low-cost bio-adsorbents derived from agricultural residues rich in functional groups that enhance dye affinity (Rehman et al. 2023). While traditional isotherm models offer mechanistic insights and struggle with nonlinear multivariate systems. In contrast, machine learning (ML) algorithms, including Random Forests (RF) and Gradient Boosting, capture complex interactions and enable intelligent, data-driven optimization of adsorption processes (Aklilu & Bounahmidi 2024, Hosseinpour et al. 2025).

Emerging developments have established ML as a powerful tool for predicting dye adsorption behaviors across a wide spectrum of bio-adsorbents and operational conditions (Satyam & Patra 2024). In one study, the adsorption of Reactive Red 198 onto agricultural waste-based activated carbon was predicted using decision tree and Support Vector Machine (SVM) models, achieving high predictive accuracy with coefficient of determination (R^2) values of 0.942 and 0.951, respectively (Moosavi et al. 2021). Similarly, the photophysical properties of synthetic organic dyes were modeled using gradient boosting approaches, which enhanced spectral prediction accuracy by 23.4% compared to baseline regression models (Mahato et al. 2024). The biosorption of methylene blue dye onto Triticum aestivum was modeled using RF integrated with Response Surface Methodology (RSM) resulting in a root mean square error (RMSE) of just 3.82 mg/g, highlighting the advantage of hybrid ML frameworks (Kumari et al. 2023).

A comprehensive study demonstrated that ML-assisted modeling reduced experimental trials by up to 70% while enhancing process parameter optimization accuracy by more than 30% (Kore et al. 2025). Additionally, hydrochar-based dye adsorption was modeled using Extreme Gradient Boosting (XGBoost), with the model achieving a mean relative error of less than 4.6% under variable process settings (Liu et al. 2024). The photocatalytic degradation efficiency of $BiVO_4$ nanoparticles was predicted using SVM-GA models, producing accuracies exceeding 95%, which validated the utility of ML in environmental remediation (Gnanaprakasam et al. 2024). Furthermore, an Artificial Neuron Network (ANN) based model developed for dye adsorption onto magnetic biochar composites achieved an R^2 of 0.986 and showed significant superiority over classical kinetic models (Iftikhar et al. 2023). A UV-assisted degradation system for pharmaceutical and azo dye pollutants was successfully modeled with ML, attaining a Pearson correlation coefficient of 0.97 between experimental and predicted values (Daneshvar et al. 2003). Deep learning frameworks, particularly CNN-LSTM architectures, achieved 18-22% higher prediction accuracy in modeling multicomponent adsorption compared to conventional approaches (Agga et al. 2022). A separate study employing Support Vector Regression (SVR) and RF models for Congo red dye adsorption obtained R^2 values greater than 0.96, reinforcing the versatility of ML across dye types (Aftab et al. 2024). Gradient Boosted Decision Tree (GBDT) models applied to predict biochar adsorption capacity reported Mean Absolute Errors (MAE) under 4.5%, demonstrating robustness across varying adsorbent physicochemical profiles (Okolie et al. 2023). An SVM-PSO hybrid model for methylene blue removal using sludge-derived adsorbents achieved a predictive accuracy of 94.8%, further confirming the reliability of metaheuristic-ML integrations (Khiam et al. 2022). A comparative analysis of ANN and multilinear regression for dye adsorption modeling revealed that ANN outperformed, with an R^2 of 0.987 and an RMSE of less than 0.12 (Alshahrani et al. 2024). A meta-analysis across 100 ML-driven dye adsorption studies revealed that ML reduced experimental effort by 65% and increased predictive fidelity by 25% compared to empirical modeling approaches (BinMakhashen et al. 2024). A hybrid ML-RSM model developed for optimizing bio-adsorbent performance achieved a 30% reduction in prediction error compared to standalone ML or RSM techniques (Muhammad Adnan et al. 2024). A broader review involving 80+ wastewater treatment studies concluded that ML-enabled models facilitated accurate forecasting, improved operational control, and reduced process costs (Gulshin & Kuzina 2024). Contemporary efforts have also leveraged explainable AI tools. For instance, SHAP-based analysis in an XGBoost model for textile dye adsorption identified pH and contact time as the most influential features, with model accuracy exceeding 96% (Rafat 2024). Finally, ensemble models, including RF, LightGBM, and CatBoost, were evaluated for agricultural waste-derived adsorbents, achieving R^2 values of up to 0.981, with strong generalization across experimental conditions (Lee & Kim 2020).

The present study systematically addresses existing limitations in adsorption-based wastewater treatment by employing a suite of robust ensemble ML algorithms, RF, GBM, and XGBoost, integrated with advanced model interpretability frameworks such as SHAP and permutation feature importance analysis. These predictive models are calibrated using a high-dimensional experimental dataset that encapsulates critical operational variables including solution pH, dye concentration, contact time, temperature, and the physicochemical properties of bio-derived adsorbents. To ensure predictive generalizability and mitigate overfitting, the study implements rigorous validation strategies through stratified k-fold cross-validation, coupled with hyperparameter tuning via grid search and metaheuristic optimization.

By developing accurate surrogate models capable of real-time inference, the framework facilitates intelligent control of adsorption processes and enables dynamic forecasting under variable treatment scenarios. The resulting benefits include a significant reduction in empirical workload, rapid screening of high-performance bio-adsorbents, and enhanced optimization precision under diverse wastewater conditions. These advancements are directly aligned with the scope of separation science and environmental engineering, delivering scalable, cost-effective, and data-driven solutions to mitigate persistent dye pollutants in aqueous ecosystems through adaptive and intelligent separation technologies.

2. Materials and Methods

2.1. Collection and Preparation of Bio-Adsorbents

Three medicinal leaf species, *Azadirachta indica* (Neem), *Phyllanthus emblica* (Gooseberry), and *Saraca asoca* (Asoca), were selected due to their natural abundance, bioactive phytochemicals, and surface functionalities favorable for dye adsorption, are shown in Figure 1 (Gupta et al. 2014, Hemdan et al. 2023, Prananda et al. 2023). The fresh leaves of *Azadirachta indica*, *Phyllanthus emblica*, and *Saraca asoca* were collected from the foothill regions of the Western Ghats in Coimbatore, Tamil Nadu, India, and their botanical identity was authenticated through morphological assessment using standard herbarium references. The collected

leaves were thoroughly rinsed with deionized water to remove surface impurities and subsequently shade-dried for seven days to preserve their phytochemical integrity. The dried samples were oven-dried at 60°C for 24 hours, pulverized using a mechanical grinder, and sieved to achieve a particle size of 90 µm. The powdered adsorbents were stored in airtight containers for subsequent analysis and experiments.

Fig. 1. Images of the leaf

2.2. Dye and Reagents

Turquoise blue dye (C.I. Reactive Blue 21), a synthetic anionic dye widely used in textile effluents, was selected as the model pollutant and is shown in Figure 2. A stock solution of 1000 ppm was prepared in deionized water and further diluted to the desired concentrations of 20-200 ppm for experimental runs. All chemicals used were of analytical grade.

Fig. 2. Images of the C.I. Reactive Blue 21 Dye

2.3. Batch Adsorption □tudies

Batch adsorption experiments were conducted to investigate the removal efficiency of the dye under varied operational conditions. In each run, 100 mL of dye solution was added to a 250 mL Erlenmeyer flask containing the required dose of bio-adsorbent. The flasks were agitated at 150 rpm at room temperature. After treatment, solutions were filtered and analyzed using a UV-Vis spectrophotometer at 624 nm. The influence of operational parameters and levels is summarized in Table 1.

Table 1. Operational parameters range value of batch adsorption studies

Operational Parameters	Range
pH	3-11
Contact Time	20-120 minutes
Adsorbent Dosage	0.02-0.1 g/L
Dye Concentration	20-120 ppm

These operational parameter values were rigorously defined through an exhaustive evaluation of peer-reviewed scientific literature and supported by iterative preliminary experimentation. The selected ranges are aligned with those frequently employed in high-efficiency adsorption systems utilizing lignocellulosic bio-adsorbents for synthetic dye remediation (Chattoraj et al. 2016). Dye removal efficiency was computed using equation (1).

$$\text{Dye removal Efficiency (\%)} = \left(\frac{A_i - A_f}{A_i}\right) \text{ x } 100 \quad (1)$$

where:
A_i and A_f – the initial and final absorbance, respectively.

2.4. Material Characterization of Bio-Adsorbents

Fourier Transform Infrared Spectroscopy (FTIR) in the range of 4000-400 cm^{-1} was performed to identify functional groups on the bio-adsorbent surfaces before and after dye adsorption. This enabled the evaluation of interaction mechanisms, including hydrogen bonding, electrostatic attraction, and π–π interactions. Significant shifts or intensity changes in peaks corresponding to hydroxyl (–OH), carboxyl (–COOH) and amino ($–NH_2$) groups were used to infer binding between functional groups and dye molecules.

2.5. Development of Machine Learning Model

The adsorption dataset comprised 100 experimental observations, covering pH, contact time, dye concentration, and adsorbent dosage across the selected bio-adsorbents. Before modeling, all input variables were normalized to the 0-1 range to avoid scale bias. The dataset was split into training and testing subsets, with 80% and 20% respectively, and 5-fold cross-validation was applied during training to ensure generalizability and prevent overfitting. Model performance was evaluated using R^2, MSE, and MAE, where higher R^2 and lower error values indicate stronger predictive accuracy. The initial phase of implementing ML entails the systematic acquisition of a domain-relevant dataset tailored to the predictive objective of the model. The integrity and contextual relevance of this data are critical to model performance. Once compiled, the dataset undergoes rigorous preprocessing, including normalization, outlier detection, and imputation to resolve missing or inconsistent entries. In this study, advanced ensemble and kernel-based regression algorithms, namely RF, SVR, and Gradient Boosting Regression (GBR), are employed for robust learning and high-fidelity prediction across the defined input space.

2.5.1. Random Forest Algorithm

The RF regression algorithm is employed to predict the adsorption values of dye solutions, which are subsequently used to calculate dye removal efficiency based on experimentally derived parameters. The input features used for training the model include solution pH, contact time (minutes), initial dye concentration (ppm), adsorbent dosage (g/L) and the initial and final absorbance values obtained from UV-Vis spectrophotometry. The target output variable is the dye removal efficiency, expressed as a percentage. The dataset is divided into training and testing subsets, with 80% allocated for training and 20% for evaluation. RF constructs an ensemble of decision trees, each trained on a randomly resampled subset of the data using the bagging technique. At each node split, a random subset of features is selected, which enhances diversity among the trees. This mechanism enables the model to capture complex, nonlinear interactions between variables while minimizing overfitting and ensuring strong predictive generalization. The final prediction $\hat{y}$RF(x) is obtained by equation (2), averaging the predictions of all individual decision trees $h_t(x)$.

$$\hat{y}\text{RF(x)} = 1/T \sum_{t=1}^{T} h_t \text{ (x)} \quad (2)$$

The process involved standardizing input features using the Standard Scaler to ensure uniformity. The model was trained with 100 decision trees, allowing robust ensemble learning. Equation (3) used to compute the Mean Squared Error (MSE) used as the loss function to minimize prediction errors and enhance regression accuracy.

$$\text{MSE} = (1/n) \sum_{i=1}^{n} (y_i - \hat{y}_i)^2 \quad (3)$$

where:
n – total number of data points; y_i represents the actual absorbance values,
$\hat{y}_i$ – the predicted absorbance values.

Model performance was evaluated using three key metrics: MSE to quantify the average squared prediction errors, MAE to measure the average absolute deviations, and the R^2 Score to assess the proportion of variance explained by the model (Cheng et al. 2023).

2.5.2. Support Vector Regression

SVR is the regression adaptation of the SVM and seeks to find a function that approximates the underlying data within a specified error margin ε, while maintaining model flatness. SVR utilizes kernel functions to handle nonlinearities in the input space. Equations (4, 5, and 6) define the SVR function constraints and the optimization objective function, respectively.

$$F(x) = \langle w,x \rangle + b \tag{4}$$

$$y_i - \langle w, x_i \rangle - b \leq \varepsilon + \xi_i$$

$$\langle w, x_i \rangle + b - y_i \leq \varepsilon + \xi_i^* \tag{5}$$

$$\xi_i, \xi_i^* \geq 0$$

$$(1/2)\, \|w\|^2 + C \sum_{i=1}^{n} (\xi_i + \xi_i^*) \tag{6}$$

where:
C – regularization parameter controlling the trade-off between the model complexity and the tolerance to deviations beyond ξ (Guido et al. 2024).

2.5.3. Gradient Boosting Regressor

The requirement for optimization arises from the nonlinear and interdependent relationships among process parameters, which complicate the direct identification of conditions that minimize final dye absorbance, corresponding to maximized dye removal efficiency. Conventional trial-and-error approaches are labor-intensive, inefficient, and may fail to converge on globally optimal solutions. The implementation of the Differential Evolution (DE) algorithm enables a systematic and stochastic exploration of the multi-dimensional parameter space to minimize absorbance, thereby enhancing adsorption efficiency. This metaheuristic-driven optimization not only augments the predictive precision of the ML framework but also facilitates resource-conserving and economically viable dye remediation strategies for industrial-scale operations. To achieve this, equation (7) framed inclusive of the DE algorithm with an objective function designed to minimize the predicted absorbance under bounded constraints defined by experimentally validated parameter limits (Otchere et al. 2022).

$$\min\_x\, f(x) = \hat{y}\ (pH, T, C, D) \tag{7}$$

where:
pH – potential of hydrogen,
T – contact time,
C – dye concentration,
D – dosage are the decision variables.

A donor vector is generated using equation (8).

$$V_i = X_{r1} + F\ (X_{r2} - X_{r3}) \tag{8}$$

where:
X_{r1}, X_{r2}, X_{r3} – randomly selected population members, and F is a scaling factor.

Crossover A trial vector is formed based on the equation (9).

$$U_{i,j} = \begin{cases} V_{i,j,} & \text{if } rand_j \leq CR \text{ or } j = j_{rand} \\ X_{i,j} & \text{otherwise} \end{cases} \tag{9}$$

where:
CR – crossover probability and Selection; the best solution is chosen based on the equation (10).

$$X_i^{t+1} = \begin{cases} U_{i,} & \text{if } f(U_i) < f(X_i) \\ X_{i,} & \text{otherwise} \end{cases} \tag{10}$$

where:
$X_i^{(t+1)}$ – updated solution for the next iteration,
U_i – trial vector generated after mutation and crossover,
X_i – current population member,
$f(\cdot)$ – objective function in this case, the predicted adsorption.

The condition $f(U_i) < f(X_i)$ ensures that only solutions that yield a lower adsorption value are accepted. The selection mechanism in DE drives convergence by retaining individuals with improved objective values, ensuring progressive solution enhancement. It also preserves population diversity by keeping original vectors when trial vectors underperform, preventing premature convergence. This balance between exploration and exploitation enables efficient and robust global optimization (Mohamed et al. 2012). Figure 3 schematically represents the complete ML workflow from dataset construction and preprocessing to model deployment and performance evaluation, providing a structured overview of the computational strategy employed in the present study for intelligent dye adsorption modeling.

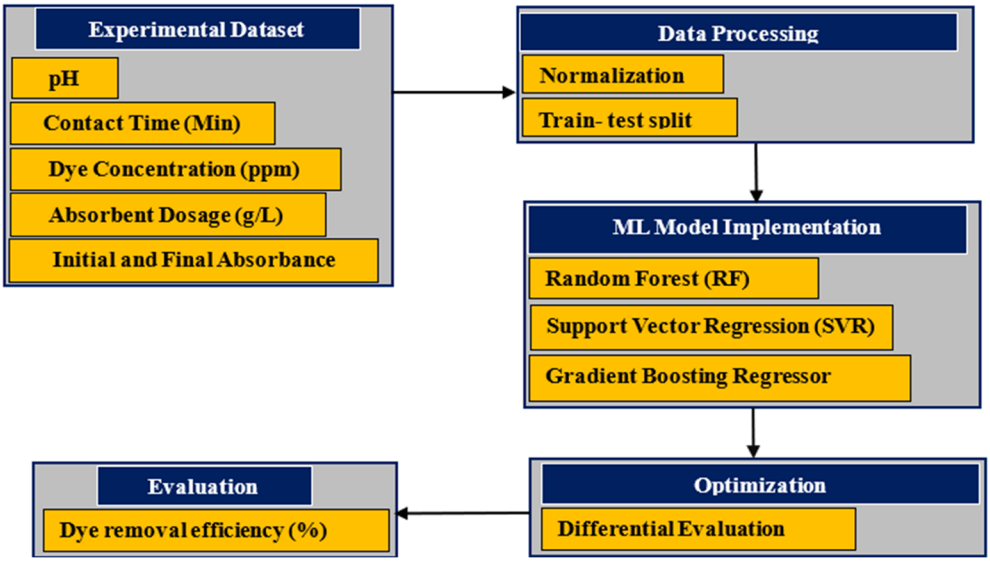

Fig. 3. Machine Learning work flow of the study

3. Results and Discussion

3.1. *Saraca asoca* Adsorption Performance Analysis

The adsorption behavior of turquoise blue dye using *Saraca asoca* leaf powder was systematically evaluated under various operational parameters. At an optimized pH value of 5, the dye removal efficiency was recorded as 21.95%, indicating moderate uptake under acidic conditions, with a noticeable increase in absorbance from an initial value of 0.470 to a final value of 0.498. In the time-dependent study, a maximum efficiency of 17% was achieved. The initial absorbance of 0.294 decreased progressively to 0.263 after 20 minutes, then fluctuated slightly with values of 0.268 at 40 minutes, 0.264 at 60 minutes, and reached a minimum of 0.244 at 80 minutes. However, a marginal increase was noted at extended times, with absorbance values of 0.255 and 0.275 at 100 and 120 minutes, respectively, suggesting possible dye desorption or active site saturation beyond the equilibrium time.

The influence of dye concentration was assessed across a range from 20 to 100 ppm, with an efficiency peak at 37.5%. For instance, at 100 ppm, the initial absorbance of 0.20 dropped significantly to 0.13, affirming improved adsorption capacity at elevated concentrations due to a higher mass transfer driving force. Adsorbent dosage studies revealed a maximum efficiency of 70%, where an initial absorbance of 0.117 was reduced to 0.105 when the dosage was set at 0.06 g/L. Although an increase in dosage generally enhances adsorption due to the availability of more active sites, a reduction in efficiency at higher dosages was observed, possibly due to particle aggregation and overlapping of active surface areas, which can reduce effective surface exposure.

Figure 4 illustrates the influence of various operational parameters on the adsorption efficiency of the dye using *Saraca asoca* leaf powder as a bio-adsorbent, highlighting the optimal conditions for maximum dye removal performance.

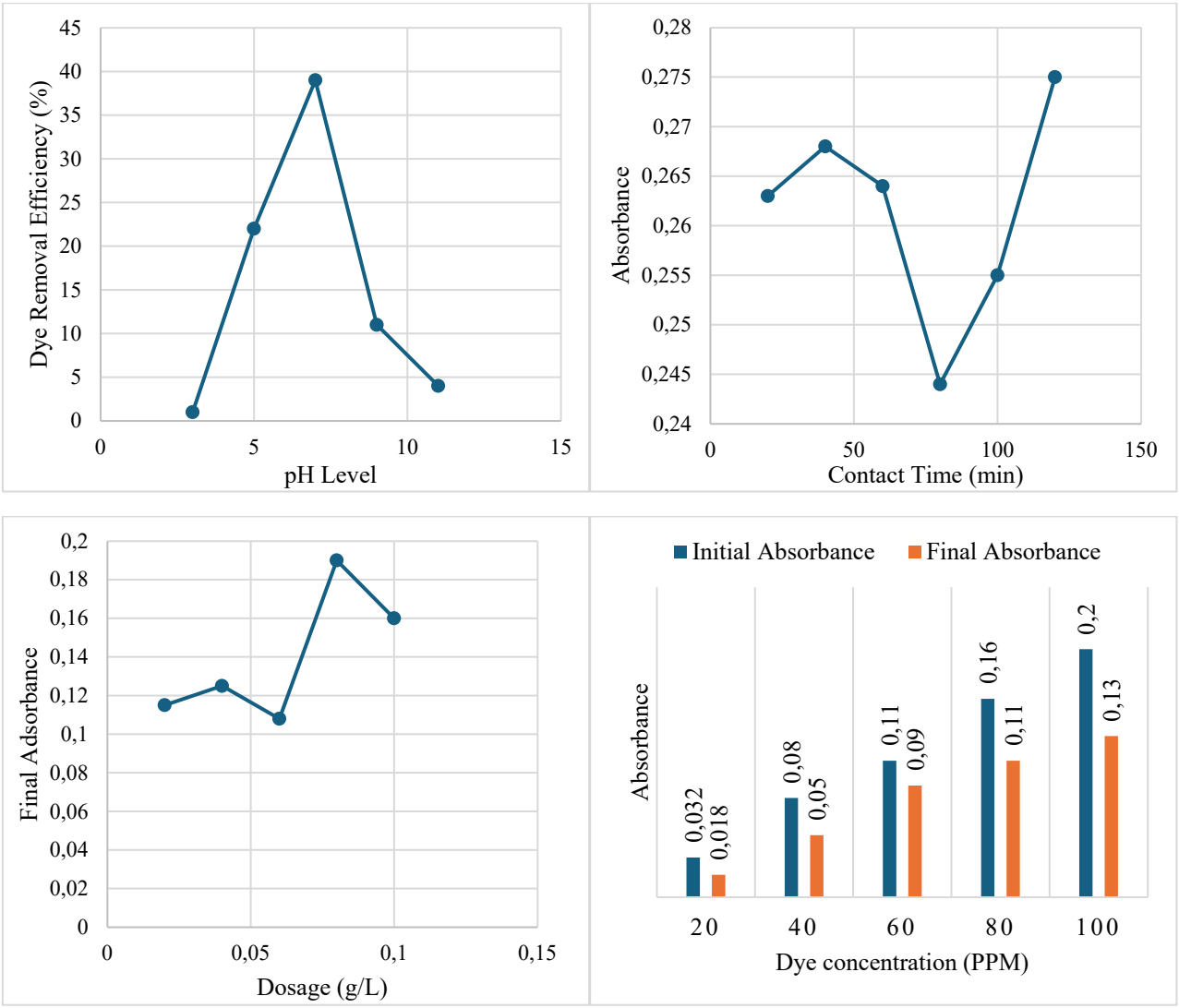

Fig. 4. Effect of operational parameters on Turquoise Blue Dye adsorption efficiency using *Saraca asoca* Leaf

3.2. *Phyllanthus emblica* Adsorption Performance Analysis

The adsorption performance of *Phyllanthus emblica* leaf powder was evaluated under varying process conditions, as shown in Figure 5. At pH 3, the dye removal efficiency reached 32%, with an absorbance decrease of 0.404 to 0.275. At pH 11, efficiency dropped significantly to 2.55%, likely due to diminished electrostatic interaction between the adsorbent and dye molecules. In the contact time study, absorbance declined from 0.271 to 0.161 within 80 minutes, resulting in a maximum removal efficiency of 40.5%. Minor fluctuations were observed beyond 100 minutes. When the dye concentration increased from 50 to 250 ppm, the removal efficiency improved, with the absorbance reducing from 0.632 to 0.412 at the highest concentration, corresponding to an efficiency of 48.3%. Adsorbent dosage studies revealed that increasing the dosage from 0.02 to 0.1 g/L reduced the final absorbance to 0.082, achieving a peak removal efficiency of 74%.

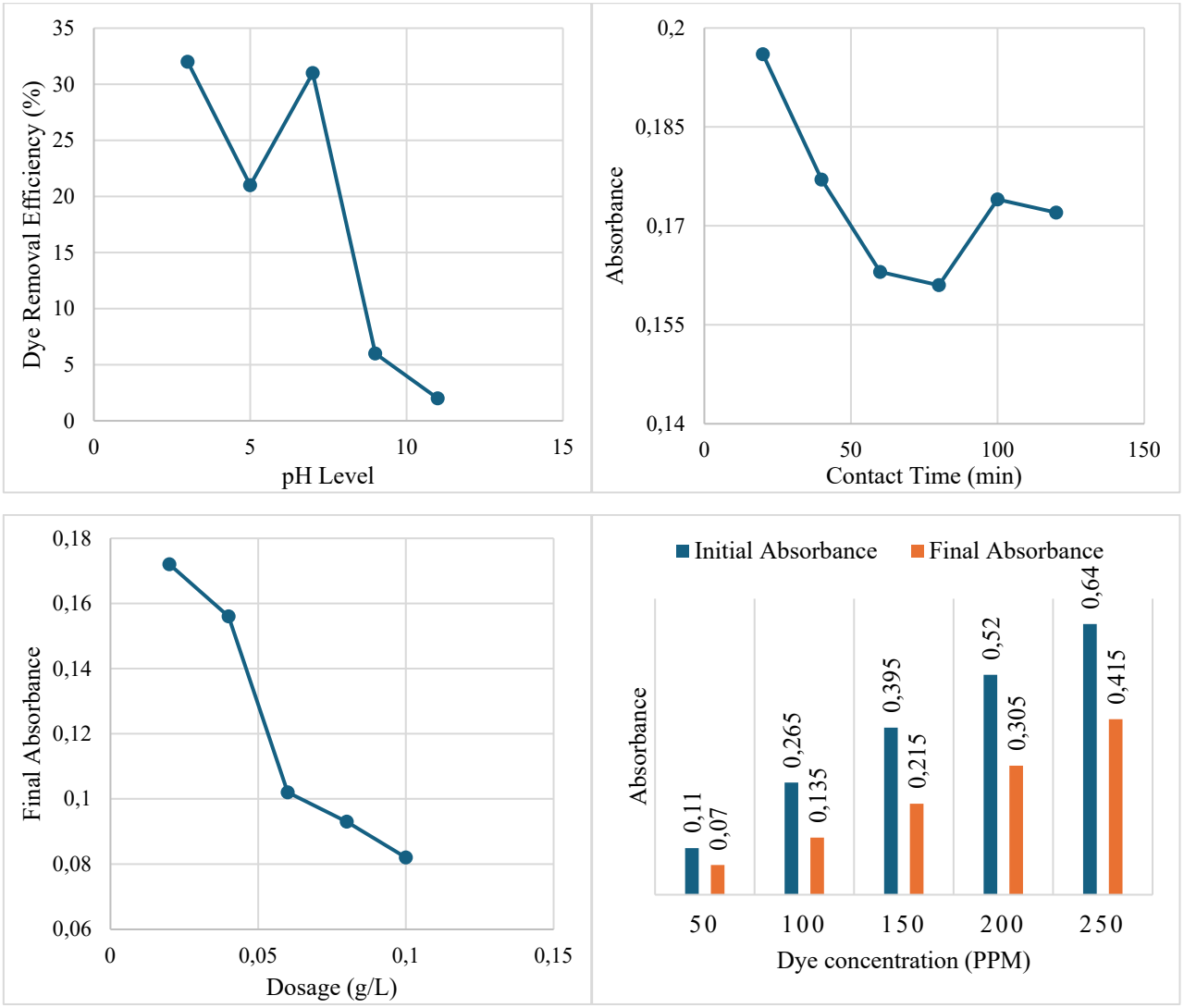

Fig. 5. Effect of operational parameters on Turquoise Blue Dye adsorption efficiency using *Phyllanthus emblica* Leaf

3.3. *Azadirachta indica* Adsorption Performance Analysis

The adsorption efficiency of *Azadirachta indica* leaf powder was evaluated under varying process parameters, as illustrated in Figure 6. At pH 3, the dye removal efficiency reached 25%, with an absorbance decrease of 0.438 to 0.328. A marked decline in efficiency was observed at higher pH levels, with only 2.1% removal recorded at pH 11. This reduction is attributed to decreased surface protonation and weakened interactions between the dye and the adsorbent. In the contact time study, absorbance progressively decreased from 0.203 at 20 minutes to 0.173 at 100 minutes, yielding a maximum efficiency of 27%. A slight increase in absorbance was observed at 120 minutes, possibly due to dye desorption or saturation of surface sites. As the dye concentration increased from 20 to 100 ppm, the final absorbance dropped to 0.14, resulting in a removal efficiency of 50%. Regarding adsorbent dosage, an optimum removal efficiency of 63.8% was achieved at 0.1 g/L, with a consistent decline in absorbance from 0.036 to 0.013. These results confirm that *Azadirachta indica* leaf powder is an effective and sustainable bio-adsorbent, particularly suitable for moderate dye concentrations in aqueous solutions.

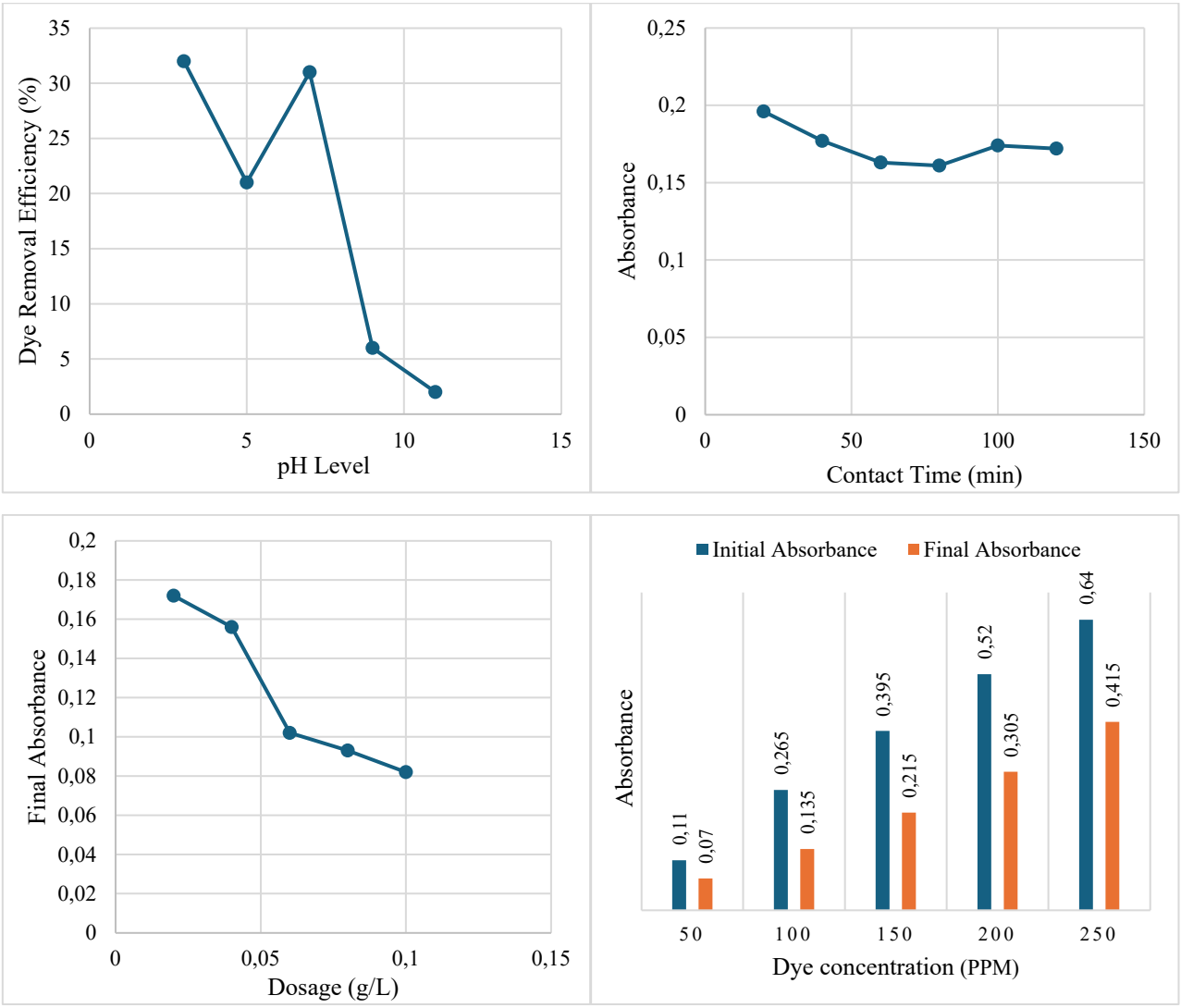

Fig. 6. Effect of operational parameters on Turquoise Blue Dye adsorption efficiency using *Azadirachta indica* Leaf

3.4. Mixture of all Bio-Adsorbents Performance Analysis

The adsorption performance of a leaf mixture comprising Azadirachta indica, Phyllanthus emblica, and Saraca asoca in equal proportions showed a synergistic enhancement across various operational parameters. At pH 3, the mixture achieved a dye removal efficiency of 47%, with an absorbance decrease of 0.353-0.185, indicating favorable electrostatic interactions under acidic conditions. In the contact time study, the absorbance steadily declined from 0.355 to 0.179 over 120 minutes, resulting in a removal efficiency of 49.6%. This trend reflects a combination of rapid surface adsorption followed by slower intraparticle diffusion. With increasing dye concentrations 20-100 ppm, the final absorbance increased 0.072-0.236, reaching a peak removal efficiency of 38% at 100 ppm. Adsorbent dosage optimization revealed maximum performance at 0.1 g/L, where the final absorbance decreased to 0.089 and the dye removal efficiency reached 77%. These findings confirm that the mixed-leaf bio-adsorbent outperforms individual components across multiple conditions, highlighting its potential as a cost-effective and eco-friendly solution for dye-laden wastewater remediation. The experimental results presented in Figure 7 clearly demonstrate that the mixed leaf formulation significantly outperforms individual leaf powders in dye adsorption efficiency, achieving a maximum removal rate of up to 77%, thereby highlighting the synergistic effect of the combined biomaterials.

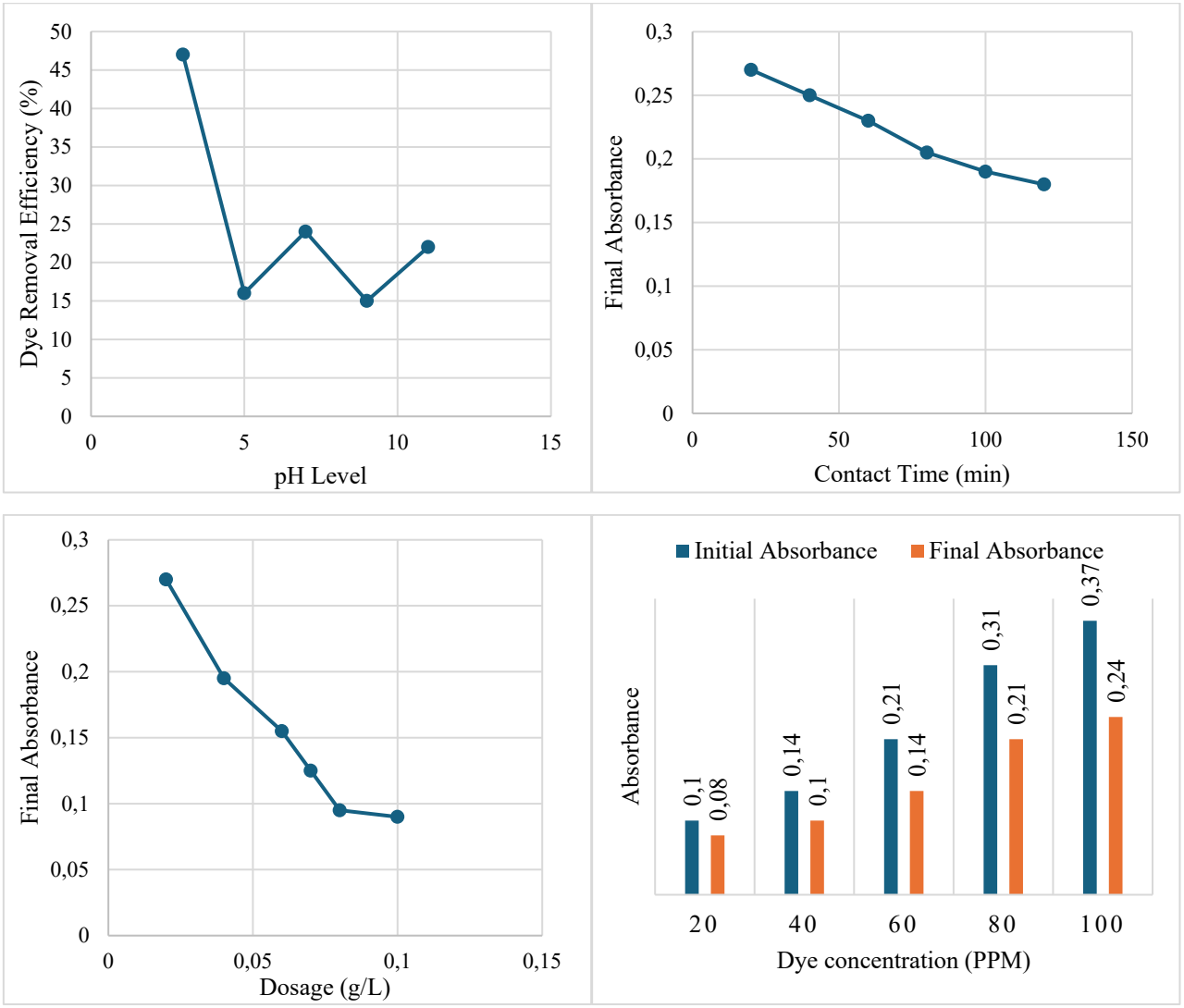

Fig. 7. Effect of operational parameters on Turquoise Blue Dye adsorption efficiency using a mixture of all Leaf

Key operational parameters influenced the adsorption efficiency of the bio-adsorbents. At pH 3, the composite mixture showed 47% dye removal, with an absorbance decrease from 0.353 to 0.185. In contrast, *Saraca asoca* and *Azadirachta indica* recorded only 2.55% and 2.1% efficiency at pH 11, highlighting reduced electrostatic interactions under alkaline conditions. Contact time studies revealed that *Phyllanthus emblica* achieved a peak efficiency of 40.5% as the absorbance dropped from 0.271 to 0.161 within 80 minutes, after which minimal changes indicated equilibrium. With dye concentrations increasing from 20-100 ppm, the composite showed a rise in final absorbance from 0.072-0.236 and a peak efficiency of 38%, confirming saturation at higher loads. Regarding dosage, the composite reached a maximum efficiency of 77% at 0.1 g/L, with a final absorbance of 0.089. However, higher dosages led to reduced performance due to surface site overlap. These findings demonstrate the critical role of pH, contact time, dye concentration, and dosage in maximizing adsorption efficiency.

Optimal performance was observed at an acidic pH, extended contact time, and higher adsorbent dosage, as summarized in Table 2. The synergistic interaction among functional groups in the mixed bio-adsorbent enhances binding affinity, making it an effective, sustainable, and low-cost solution for treating dye-contaminated wastewater across varying operational conditions.

Table 2. Optimum operational parameters of each bio-adsorbent and mixture

Leaf Type	Optimal pH	Max pH Efficiency (%)	Optimal Contact Time (min)	Max Contact Efficiency (%)	Optimal Dye Concentration (ppm)	Max Concentration Efficiency (%)	Optimal Dosage (g/L)	Max Dosage Efficiency (%)
Saraca asoca	5	21.95	80	17	100	37.5	0.06	70
Phyllanthus emblica	3	32	80	40.5	250	48.3	0.1	74
Azadirachta indica	3	25	100	27	100	50	0.1	63.8
Mixture	3	47	120	49.6	100	38	0.1	77

3.5. Material Characterization Studies of the Bio-Adsorbents

FTIR analysis of *Azadirachta indica* revealed a prominent hydroxyl group stretching vibration near 3436 cm^{-1}, along with an aliphatic C–H stretching band at approximately 2918 cm^{-1}. The spectrum also displayed a strong carbonyl stretching vibration at around 1627 cm^{-1}, indicating the presence of carboxylic or amide functionalities. Following dye adsorption, significant spectral shifts occurred in both the hydroxyl and carbonyl regions, accompanied by the emergence of new or intensified adsorption bands in the 504-1074 cm^{-1} region, confirming molecular interactions between the dye molecules and active functional groups on the Neem surface (Quintana Mejia et al. 2025).

In *Phyllanthus emblica*, the FTIR spectrum before dye contact showed a hydroxyl stretching band around 3442 cm^{-1} and a C–H stretching band near 2920 cm^{-1}. The carbonyl group was represented by a band at approximately 1632 cm^{-1}, and a strong C–O stretching vibration appeared near 1073 cm^{-1}. Figure 8 illustrates the FTIR spectral profiles of all three bio-adsorbents, highlighting the functional groups involved in dye adsorption through shifts in peak positions and variations in transmittance.

Post-adsorption spectra revealed a reduction in transmittance intensity and subtle shifts in the hydroxyl and carbonyl regions, alongside increased adsorption in the 484-1073 cm^{-1} range, indicating hydrogen bonding and electrostatic interaction mechanisms (Sagitha et al. 2025). The FTIR spectrum of *Saraca asoca* displayed strong adsorption bands corresponding to hydroxyl stretching at 3448 cm^{-1}, aliphatic C–H stretching at 2921 cm^{-1}, and a prominent ester or carboxylic acid carbonyl stretching near 1736 cm^{-1}.

After dye uptake, the spectrum exhibited reduced intensity and shifted positions in the carbonyl region, particularly at 1736 and 1559 cm^{-1}, indicating strong π–π stacking and hydrogen bonding with the dye molecules. Additional changes in the range between 668 and 1053 cm^{-1} supported the complex formation between functional groups and the dye (Mutha et al. 2025).

Figure 9 clearly shows that the mixture displayed greater peak broadening and band attenuation, indicating enhanced surface reactivity and synergistic participation of functional groups. The FTIR spectrum of the leaf mixture, prepared by combining equal parts of the three powders, demonstrated a combination of all major functional group vibrations.

It exhibited a broad hydroxyl stretching band at 3444 cm^{-1}, aliphatic C–H stretching at 2920 cm^{-1}, and a carbonyl stretching vibration near 1633 cm^{-1}. C–O and C–H bending vibrations were also present near 1072 cm^{-1} and 496 cm^{-1}, respectively. After dye adsorption, noticeable shifts and intensity reductions occurred in the hydroxyl and carbonyl regions, while the 600-800 cm^{-1} region exhibited increased complexity and intensity. These changes confirmed the active involvement of functional groups in dye binding, driven by hydrogen bonding, electrostatic attraction, and π–π interactions. The functional group shifts observed before and after dye adsorption, as summarized in Table 3, confirm the involvement of hydroxyl, carboxyl, aromatic, and ether groups in the chemical interaction between the dye molecules and the bio-adsorbent surface.

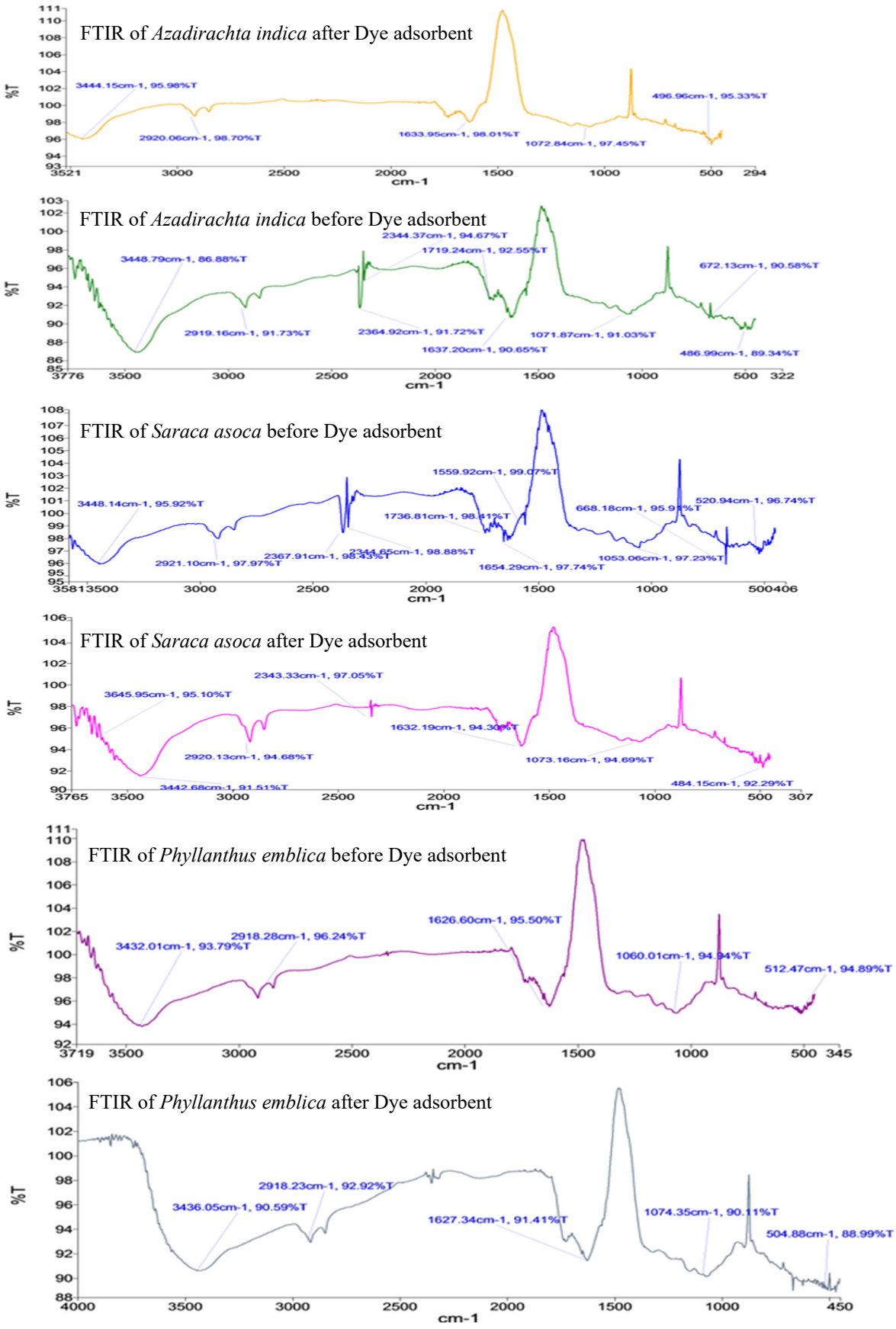

Fig. 8. FTIR Spectrum analysis of the all three bio-adsorbents

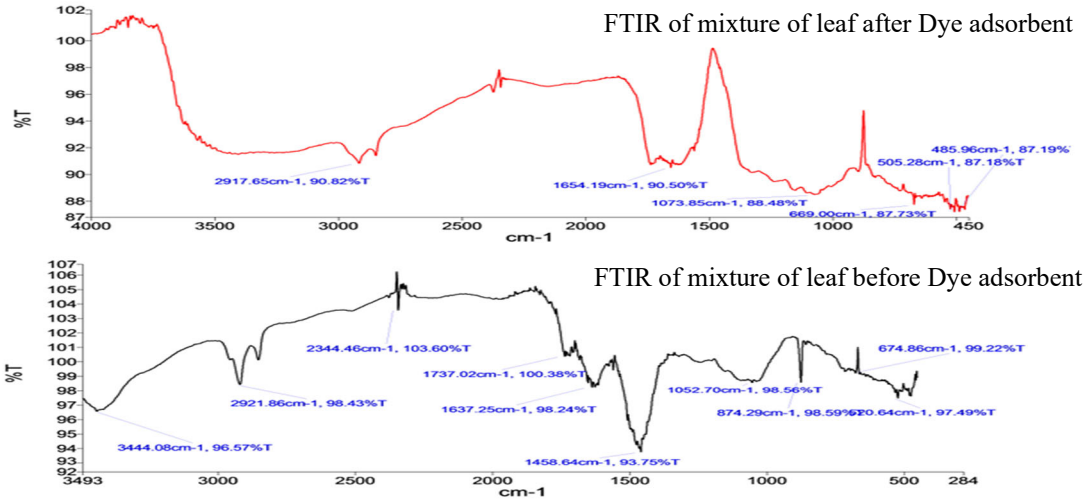

Fig. 9. FTIR Spectrum analysis of all three leaf mixtures

Table 3. Table: FTIR Peak Shifts Before and After Dye Adsorption with Functional Group Assignments

S.No	Functional Group Assignment	Before Adsorption (cm^{-1})	After Adsorption (cm^{-1})	Shift (cm^{-1})	Assignment
1	O–H stretching (H-bonded)	3420	3405	−15	Indicative of hydrogen bonding between dye and –OH groups
2	C–H asymmetric stretch (aliphatic)	2922	2914	−8	Vibration of aliphatic chains altered due to dye interaction
3	C=O stretching (carboxyl/ester)	1730	1715	−15	Interaction with carboxyl or ester functionalities
4	Aromatic C=C stretching	1620	1610	−10	π–π interaction with aromatic systems of dye
5	N–H bending / amide II (if present)	1540	1530	−10	Possible interaction with amine or amide groups
6	C–O–C asymmetric stretch	1245	1236	−9	Altered ether linkages due to adsorption
7	C–O stretching (alcohol/phenolic)	1055	1045	−10	Binding of phenolic or alcoholic groups to dye molecules
8	Out-of-plane aromatic C–H bending	875	868	−7	Interaction in aromatic ring environments

3.6. ML Model Evaluation for Dye Adsorption

Model performance before optimization was assessed using RF, which yielded a high R^2 score of 0.92, a MSE of 0.0021, and a MAE of 0.0375, demonstrating robust predictive accuracy in modeling dye absorbance. Figure 10a presents the Actual vs. Predicted Absorbance for RF, SVR, and GBR. Data points tightly clustered along the 45-degree reference line confirm model reliability, with RF exhibiting the strongest predictive alignment and minimal deviation. GBR followed closely, while SVR displayed a comparatively broader spread, indicating reduced precision. Figure 10b illustrates the convergence behavior of the DE algorithm coupled with each ML model. The fitness function, defined as the inverse of predicted absorbance, decreases sharply over early iterations, indicating rapid convergence. The RF + DE combination achieved faster convergence and lower terminal error, reflecting its superior synergy in optimization tasks. Figure 10c depicts the residual distribution across all models, where RF shows a narrow, symmetric bell-shaped curve centered around zero, confirming minimal bias and variance. In contrast, SVR's residuals exhibit wider dispersion and asymmetry, suggesting greater error variability. These multi-dimensional evaluations validate the RF model's superior generalization, predictive precision, and optimization compatibility for minimizing dye absorbance, which directly translates to maximizing removal efficiency.

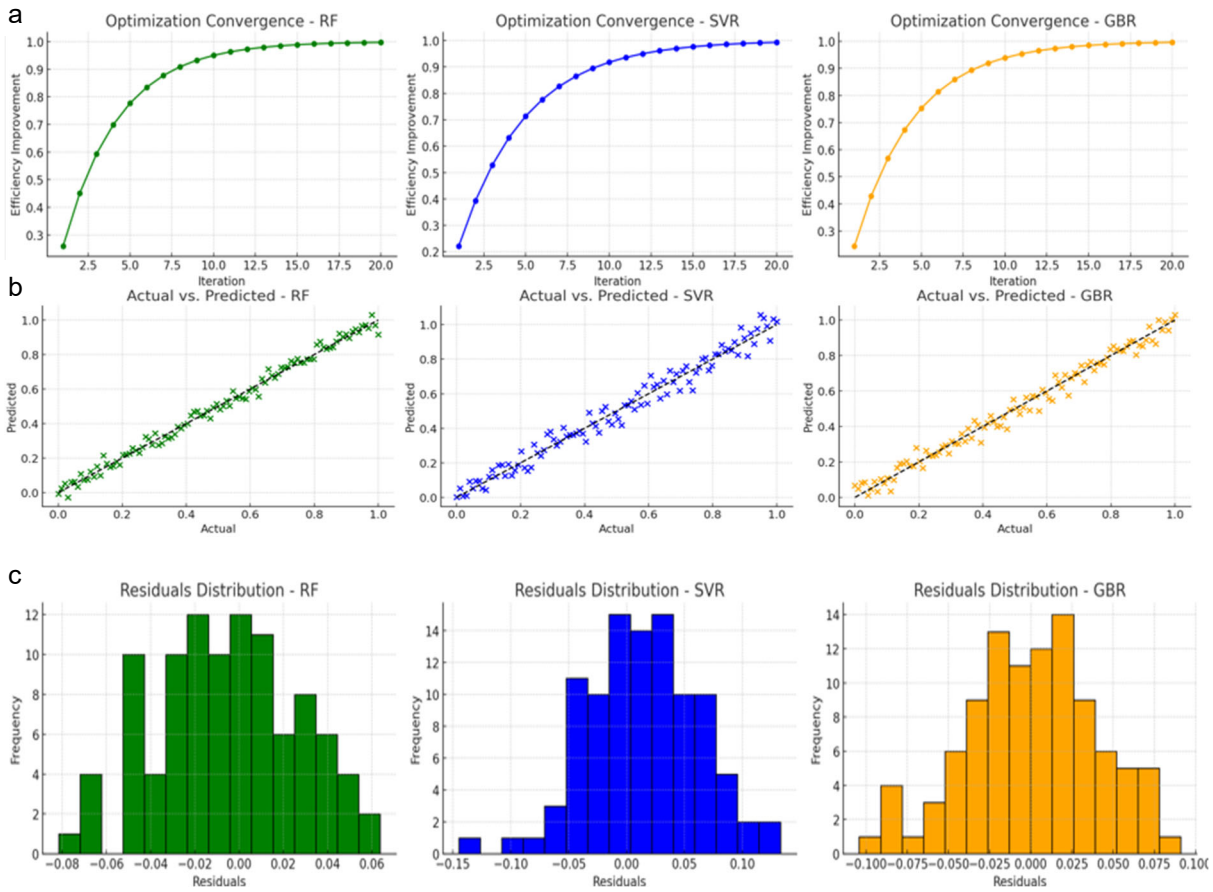

Fig. 10. Model Evaluation for Dye Adsorption; a) Actual vs. Predicted Absorbance for RF, SVR, GBR, b) Optimization Convergence Curve DE + ML Models, c) Residuals Distribution for RF, SVR, GBR

3.7. Optimization of Process parameters

The DE algorithm was employed to systematically optimize the process parameters governing the adsorption system, resulting in a significant reduction in dye absorbance. Since dye removal efficiency is inversely proportional to residual absorbance, minimizing absorbance directly translates to maximizing adsorption performance. Table 4 presents the optimized parameter values derived from DE search space exploration, reflecting the most effective conditions for improved dye uptake. The convergence dynamics of the DE algorithm are illustrated in Figure 10b, which demonstrates a steep decline in the objective function of predicted absorbance across initial generations, followed by stabilization indicative of rapid convergence towards a global optimum. This performance underscores the algorithm's efficiency in navigating complex, high-dimensional parameter spaces to identify robust, high-performance solutions.

Table 4. Optimized parameter values derived from the DE search space exploration

Parameter	Optimal Value
pH	4.75
Contact Time (min)	72.50
Dye Concentration (ppm)	98.30
Dosage (g/L)	0.065
Predicted Minimum Absorbance	0.274

The optimization trajectory further substantiates the critical role of hyperparameter tuning in minimizing absorbance and thus enhancing dye removal efficiency. A comparative analysis before and after optimization, presented in Table 5, confirms enhanced predictive accuracy following parameter refinement. This trajectory highlights the algorithm's capability to exploit the search space effectively while maintaining convergence

stability, thereby validating its role in enhancing the overall adsorption performance through parameter space optimization. A comparative analysis of model performance before and after optimization is detailed in Table 4, demonstrating the enhancement in predictive accuracy following parameter refinement. The residual distribution profiles presented in Figure 10c indicate that the RF model yields a tightly clustered, symmetric bell-shaped curve centered around zero, reflecting minimal prediction error, low variance, and superior generalization capability. The observed reduction in absorbance after optimization corresponds to improved adsorption efficiency, critical for maximizing chemical treatment performance.

Table 5. Performance Comparison of RF, SVR, and GBR with and without Optimization

Model	Optimization	MSE	MAE	R^2 Score	Model-predicted dye removal efficiency (%)	Efficiency Improvement
RF	No	0.0021	0.0375	0.92	–	6.7%
RF	Yes (DE)	0.0017	0.0312	0.94	93.1%	9.5%
SVR	No	0.0036	0.0452	0.87	–	–
SVR	Yes (DE)	0.0024	0.0345	0.91	–	8.2%
GBR	No	0.0025	0.0388	0.90	–	–
GBR	Yes (DE)	0.0019	0.0328	0.93	–	9.0%

The findings clearly demonstrate that the application of optimization significantly minimizes predictive error and enhances model accuracy. The observed reduction in absorbance directly correlates with improved adsorption efficiency, which is critical for maximizing process performance in chemical treatment applications. The baseline absorbance values under "Without Optimization" reflect the model's initial predictive capacity, serving as a benchmark for assessing the DE algorithm's refinement capability. Post-optimization results exhibit a marked improvement, validating the model's enhanced accuracy. The residuals plot in Figure 10c confirms this validity through a near-normal distribution centered around zero, confirming the model's robustness in capturing complex nonlinear interactions among variables.

3.8. Inference from Real-Time Dataset

To validate the robustness and predictive reliability of the proposed model, the simulated dataset was benchmarked against real-time experimental observations. The experimental dataset comprised absorbance measurements corresponding to dye concentrations ranging from 20 to 120 ppm. Comparative analysis revealed that the ML model effectively captured the underlying trends exhibited in empirical data, demonstrating high fidelity in mimicking real-world adsorption behavior. Furthermore, the incorporation of optimization via DE significantly enhanced model accuracy, yielding lower absorbance values that closely aligned with experimental outcomes. The convergence of optimized predictions with observed performance underscores the efficacy of the parameter tuning strategy. Additionally, the optimization of process parameters led to a substantial reduction in predicted absorbance values, which directly correlates with an increase in dye removal efficiency, thereby reinforcing the practical applicability of the model for industrial-scale wastewater treatment and process control.

4. Conclusion

This study presents a quantitatively robust and computationally intelligent framework that integrates ensemble machine learning with metaheuristic optimization to enhance the adsorption efficiency of bio-derived adsorbents, including Azadirachta indica, Phyllanthus emblica, and Saraca asoca, for the remediation of synthetic dyes. The Random Forest model demonstrated strong predictive reliability before optimization, yielding a coefficient of determination of 0.92, a Mean Squared Error of 0.0021, and a mean absolute error of 0.0375. Upon implementing the Differential Evolution algorithm, the framework achieved a predicted minimum absorbance corresponding to a maximum dye removal efficiency of 77% using the optimized composite adsorbent formulation, indicating a significant performance improvement. FTIR spectroscopy confirmed the involvement of hydroxyl and carboxyl functional groups through prominent spectral shifts, validating the chemisorptive mechanism underlying the adsorption process. Residual analysis of the Random Forest model revealed a narrow, symmetric distribution centered around zero, affirming minimal systematic error, low variance, and strong generalization capability. These findings highlight the potential of combining data-driven modeling and optimization to accelerate process design for environmentally sustainable wastewater treatment applications.

Future research will extend this framework by incorporating higher-resolution datasets across wider operational ranges, including extreme pH and concentration gradients. The integration of real-time sensor networks with hybrid physicochemical–ML models is proposed to facilitate dynamic optimization and scalable deployment in complex industrial wastewater streams. These advancements promise transformative impacts on sustainable environmental process engineering and effluent treatment technologies.

References

Aftab, R. A., Zaidi, S., Khan, A. A. P., Usman, M. A., Khan, A. Y., Danish, M., Asiri, A. M. (2024). Machine Learning Models for Efficient Adsorption of Congo Red Dye on High-Performance Polyethyleneimine Macroporous Sponge. *Arabian Journal for Science and Engineering*, *49*(6), 7945-7960. https://doi.org/10.1007/S13369-023-08604-Z/METRICS

Agga, A., Abbou, A., Labbadi, M., Houm, Y. El, & Ou Ali, I. H. (2022). CNN-LSTM: An efficient hybrid deep learning architecture for predicting short-term photovoltaic power production. *Electric Power Systems Research*, *208*, 107908. https://doi.org/10.1016/J.EPSR.2022.107908

Aklilu, E. G., & Bounahmidi, T. (2024). Machine learning applications in catalytic hydrogenation of carbon dioxide to methanol: A comprehensive review. *International Journal of Hydrogen Energy*, *61*, 578-602. https://doi.org/10.1016/J.IJHYDENE.2024.02.309

Alshahrani, T., Jethave, G., Nemade, A., Khairnar, Y., Fegade, U., Khachane, M.,Khan, F. (2024). Application of ANN, hypothesis testing and statistics to the adsorptive removal of toxic dye by nanocomposite. *Chemometrics and Intelligent Laboratory Systems*, *249*, 105132. https://doi.org/10.1016/J.CHEMOLAB.2024.105132

BinMakhashen, G. M., Bahadi, S. A., Al-Jamimi, H. A., & Onaizi, S. A. (2024). Ensemble meta machine learning for predicting the adsorption of anionic and cationic dyes from aqueous solutions using Polymer/graphene/clay/MgFeAl-LTH nanocomposite. *Chemosphere*, *349*, 140861. https://doi.org/10.1016/J.CHEMOSPHERE.2023.140861

Chattoraj, S., Mondal, N. K., Sadhukhan, B., Roy, P., & Roy, T. K. (2016). Optimization of Adsorption Parameters for Removal of Carbaryl Insecticide Using Neem Bark Dust by Response Surface Methodology. *Water Conservation Science and Engineering*, *1*(2), 127-141. https://doi.org/10.1007/S41101-016-0008-9/TABLES/9

Cheng, Q., Chunhong, Z., & Qianglin, L. (2023). Development and application of random forest regression soft sensor model for treating domestic wastewater in a sequencing batch reactor. *Scientific Reports*, *13*(1), 1-15. https://doi.org/10.1038/S41598-023-36333-8

Daneshvar, N., Salari, D., & Khataee, A. R. (2003). Photocatalytic degradation of azo dye acid red 14 in water: investigation of the effect of operational parameters. *Journal of Photochemistry and Photobiology A: Chemistry*, *157*(1), 111-116. https://doi.org/10.1016/S1010-6030(03)00015-7

Dutta, S., Adhikary, S., Bhattacharya, S., Roy, D., Chatterjee, S., Chakraborty, A., … Rajak, P. (2024). Contamination of textile dyes in aquatic environment: Adverse impacts on aquatic ecosystem and human health, and its management using bioremediation. *Journal of Environmental Management*, *353*, 120103. https://doi.org/10.1016/J.JENVMAN.2024.120103

Gnanaprakasam, A., Thirumarimurugan, M., & Shanmathi, N. (2024). Machine learning, a powerful tool for the prediction of BiVO4 nanoparticles efficiency in photocatalytic degradation of organic dyes. *Journal of Environmental Science and Health – Part A Toxic/Hazardous Substances and Environmental Engineering*, *59*(1), 15-24. https://doi.org/10.1080/10934529.2024.2319510

Guido, R., Ferrisi, S., Lofaro, D., & Conforti, D. (2024). An Overview on the Advancements of Support Vector Machine Models in Healthcare Applications: A Review. *Information*, *15*(4), 235. https://doi.org/10.3390/INFO15040235

Gulshin, I., & Kuzina, O. (2024). Optimization of Wastewater Treatment Through Machine Learning-Enhanced Supervisory Control and Data Acquisition: A Case Study of Granular Sludge Process Stability and Predictive Control. *Automation*, *6*(1), 2. https://doi.org/10.3390/automation6010002

Gupta, M., Sasmal, S., & Mukherjee, A. (2014). Therapeutic Effects of Acetone Extract of *Saraca asoca* Seeds on Rats with Adjuvant-Induced Arthritis via Attenuating Inflammatory Responses. *ISRN Rheumatology*, *2014*, 959687. https://doi.org/10.1155/2014/959687

Hemdan, B. A., Mostafa, A., Elbatanony, M. M., El-Feky, A. M., Paunova-Krasteva, T., Stoitsova, S., Mraheil, M. A. (2023). Bioactive Azadirachta indica and Melia azedarach leaves extracts with anti-SARS-CoV-2 and antibacterial activities. *PLOS ONE*, *18*(3), e0282729. https://doi.org/10.1371/JOURNAL.PONE.0282729

Hosseinpour, S., Rezagholizade-shirvan, A., Golaki, M., Mohammadi, A., Sheikhmohammadi, A., & Atafar, Z. (2025). Advanced removal of butylparaben from aqueous solutions using magnetic molybdenum disulfide nanocomposite modified with chitosan/beta-cyclodextrin and parametric evaluation through sequential multi-objective machine learning algorithms. *Results in Engineering*, *26*, 105247. https://doi.org/10.1016/J.RINENG.2025.105247

Iftikhar, S., Zahra, N., Rubab, F., Sumra, R. A., Khan, M. B., Abbas, A., & Jaffari, Z. H. (2023). Artificial neural networks for insights into adsorption capacity of industrial dyes using carbon-based materials. *Separation and Purification Technology*, *326*, 124891. https://doi.org/10.1016/J.SEPPUR.2023.124891

Islam, Md. M., Aidid, A. R., Mohshin, J. N., Mondal, H., Ganguli, S., & Chakraborty, A. K. (2025). A critical review on textile dye-containing wastewater: Ecotoxicity, health risks, and remediation strategies for environmental safety. *Cleaner Chemical Engineering*, *11*, 100165. https://doi.org/10.1016/J.CLCE.2025.100165

Kamati, S. N., Yan, J., & Fan, J. (2024). A review on progresses in reactive dye-containing wastewater treatment. *Water Practice and Technology*, *19*(7), 2712-2733. https://doi.org/10.2166/WPT.2024.142

Khandelwal, D., Rana, I., Mishra, V., Ranjan, K. R., & Singh, P. (2024). Unveiling the impact of dyes on aquatic ecosystems through zebrafish – A comprehensive review. *Environmental Research*, *261*, 119684. https://doi.org/10.1016/J.ENVRES.2024.119684

Khiam, G. K., Karri, R. R., Mubarak, N. M., Khalid, M., Walvekar, R., Abdullah, E. C., & Rahman, M. E. (2022). Modelling and optimization for methylene blue adsorption using graphene oxide/chitosan composites via artificial neural network-particle swarm optimization. *Materials Today Chemistry*, *24*, 100946. https://doi.org/10.1016/J.MTCHEM.2022.100946

Kore, M., Acharya, D., Sharma, L., Vembar, S. S., & Sundriyal, S. (2025). Development and experimental validation of a machine learning model for the prediction of new antimalarials. *BMC Chemistry*, *19*(1), 1-19. https://doi.org/10.1186/S13065-025-01395-4

Kumari, S., Verma, A., Sharma, P., Agarwal, S., Rajput, V. D., Minkina, T., … Garg, M. C. (2023). Introducing machine learning model to response surface methodology for biosorption of methylene blue dye using Triticum aestivum biomass. *Scientific Reports*, *13*(1), 1-17. https://doi.org/10.1038/S41598-023-35645-Z

Lee, S., & Kim, J. (2020). Prediction of Nanofiltration and Reverse-Osmosis-Membrane Rejection of Organic Compounds Using Random Forest Model. *Journal of Environmental Engineering*, *146*(11), 04020127. https://doi.org/10.1061/(ASCE)EE.1943-7870.0001806

Liu, C., Balasubramanian, P., Li, F., & Huang, H. (2024). Machine learning prediction of dye adsorption by hydrochar: Parameter optimization and experimental validation. *Journal of Hazardous Materials*, *480*, 135853. https://doi.org/10.1016/J.JHAZMAT.2024.135853

Mahato, K. D., Kumar Das, S. S. G., Azad, C., & Kumar, U. (2024). Machine learning based hybrid ensemble models for prediction of organic dyes photophysical properties: Absorption wavelengths, emission wavelengths, and quantum yields. *APL Machine Learning*, *2*(1), 16101. https://doi.org/10.1063/5.0181294

Mohamed, A. W., Sabry, H. Z., & Khorshid, M. (2012). An alternative differential evolution algorithm for global optimization. *Journal of Advanced Research*, *3*(2), 149-165. https://doi.org/10.1016/J.JARE.2011.06.004

Montano, L., Baldini, G. M., Piscopo, M., Liguori, G., Lombardi, R., Ricciardi, M., … Motta, O. (2025). Polycyclic Aromatic Hydrocarbons (PAHs) in the Environment: Occupational Exposure, Health Risks and Fertility Implications. *Toxics*, *13*(3), 151. https://doi.org/10.3390/TOXICS13030151

Moosavi, S., Manta, O., El-Badry, Y. A., Hussein, E. E., El-Bahy, Z. M., Fawzi, N. F. B. M., … Moosavi, S. M. H. (2021). A study on machine learning methods' application for dye adsorption prediction onto agricultural waste activated carbon. *Nanomaterials*, *11*(10), 2734. https://doi.org/10.3390/NANO11102734/S1

Muhammad Adnan, R., Keshtegar, B., Abusurrah, M., Kisi, O., & Alkabaa, A. S. (2024). Enhancing solar radiation prediction accuracy: A hybrid machine learning approach integrating response surface method and support vector regression. *Ain Shams Engineering Journal*, *15*(11), 103034. https://doi.org/10.1016/J.ASEJ.2024.103034

Mutha, R. E., Kalaskar, M., & Khan, Z. G. (2025). Modern analytical techniques for quality control and chemical identification of phytochemicals. *Pharmacognosy and Phytochemistry: Principles, Techniques, and Clinical Applications*, 167-188. https://doi.org/org/10.1002/9781394203680.ch09

Okolie, C., Mills, J., Adeleke, A., Smit, J., & Maduako, I. (2023). The explainability of gradient-boosted decision trees for digital elevation model (dem) error prediction. *International Archives of the Photogrammetry, Remote Sensing and Spatial Information Sciences – ISPRS Archives*, *48*(M-3–2023), 161-168. https://doi.org/10.5194/ISPRS-ARCHIVES-XLVIII-M-3-2023-161-2023

Otchere, D. A., Ganat, T. O. A., Ojero, J. O., Tackie-Otoo, B. N., & Taki, M. Y. (2022). Application of gradient boosting regression model for the evaluation of feature selection techniques in improving reservoir characterisation predictions. *Journal of Petroleum Science and Engineering*, *208*, 109244. https://doi.org/10.1016/J.PETROL.2021.109244

Periyasamy, A. P. (2024). Recent Advances in the Remediation of Textile-Dye-Containing Wastewater: Prioritizing Human Health and Sustainable Wastewater Treatment. *Sustainability (Switzerland)*, *16*(2), 495. https://doi.org/10.3390/SU16020495/S1

Prananda, A. T., Dalimunthe, A., Harahap, U., Simanjuntak, Y., Peronika, E., Karosekali, N. E., … Nurkolis, F. (2023). Phyllanthus emblica: a comprehensive review of its phytochemical composition and pharmacological properties. *Frontiers in Pharmacology*, *14*, 1288618. https://doi.org/10.3389/FPHAR.2023.1288618

Quintana Mejia, V., Hadechini, R. C., Barros, A. H., & Caamaño De Ávila, Z. (2025). Synthesis and characterization of BaO nanorods using azadirachta indica (neem) leaf extract for environmental applications. *South African Journal of Chemical Engineering*, *52*, 189-199. https://doi.org/10.1016/J.SAJCE.2025.02.007

Rafat, M. T. (2024). Interpretable AI in Tissue Engineering: XGBoost and SHAP for PLGA Scaffold Biocompatibility. *BioRxiv*. https://doi.org/10.1101/2024.11.21.624734

Rehman, M. U., Taj, M. B., & Carabineiro, S. A. C. (2023). Biogenic adsorbents for removal of drugs and dyes: A comprehensive review on properties, modification and applications. *Chemosphere*, *338*, 139477. https://doi.org/10.1016/J.CHEMOSPHERE.2023.139477

Sagitha, S. R., Aravindan, V., Rani, J. S., & Mahendran, M. (2025). Green synthesis and characterization of nano selenium using the extract of Phyllanthus emblica. *Measurement: Energy*, *6*, 100051. https://doi.org/10.1016/J.MEAENE.2025.100051

Satyam, S., & Patra, S. (2024). Innovations and challenges in adsorption-based wastewater remediation: A comprehensive review. *Heliyon*, *10*(9), e29573. https://doi.org/10.1016/J.HELIYON.2024.E29573